Isothermal and Isobaric Desorption of Carbon Dioxide by Purge

ARTICLE *in* INDUSTRIAL & ENGINEERING CHEMISTRY RESEARCH · AUGUST 1995

Impact Factor: 2.59 · DOI: 10.1021/ie00047a042

2 AUTHORS, INCLUDING:

Timothy C. Golden
Air Products and Chemicals. Inc.
34 PUBLICATIONS **852** CITATIONS

SEE PROFILE

Isothermal and Isobaric Desorption of Carbon Dioxide by Purge

Shivaji Sircar, and Timothy C. Golden

Ind. Eng. Chem. Res., **1995**, 34 (8), 2881-2888• DOI: 10.1021/ie00047a042 • Publication Date (Web): 01 May 2002

Isothermal and Isobaric Desorption of Carbon Dioxide by Purge

Shivaji Sircar* and Timothy C. Golden

Air Products and Chemicals, Inc. 7201 Hamilton Boulevard, Allentown, Pennsylvania 18195

Isothermal and isobaric desorption of carbon dioxide was experimentally evaluated by purging adsorbent columns saturated with pure carbon dioxide with pure hydrogen, nitrogen, and methane. Three different activated carbons and two zeolites were investigated as adsorbents. The effects of purge gas flow rate, system pressure and temperature, strength of carbon dioxide adsorption, and selectivity of adsorption between carbon dioxide and the purge gas on the desorption process were measured. Instantaneous local equilibrium between gas and adsorbed phases was established under the conditions of the experiments. An analytical mathematical model for isothermal and isobaric desorption of binary gas mixtures by purge was developed. It was demonstrated that the efficiency of desorption by purge can be increased by (1) lowering the desorption pressure, (2) increasing the adsorbent temperature, and (3) increasing the selectivity of adsorption of the purge gas over the desorbing component.

Introduction

Adsorption and desorption constitute the two most basic steps in all pressure swing adsorption (PSA) processes for gas separation. They are used in conjunction with many other complementary steps (which are designed to enhance the separation efficiency) in a PSA process (Sircar, 1989a). The adsorption step is a thermodynamically spontaneous process. It is achieved by merely contacting the more selectively adsorbed components of a feed gas mixture with the adsorbent as long as the partial pressures of these components in the feed gas are larger than the corresponding gas phase partial pressures in equilibrium with the respective adsorbate loadings in the adsorbent. The desorption steps, on the other hand, are the primary energy-consuming steps in the PSA process. They also dictate the overall separation efficiency.

The desorption of the selectively adsorbed components is usually achieved by (a) reduction of total gas phase pressure (depressurization) over the adsorbent which can decrease the superincumbent gas phase partial pressure of the adsorbates and (b) reduction of superincumbent gas phase partial pressures of the adsorbates by flowing a less selectively adsorbed gas (purging) at a constant total gas pressure over the adsorbent.

Energy is consumed during the depressurization step in the form of (a) loss of feed gas pressure energy when the adsorption step is carried out at a superatmospheric pressure level and (b) mechanical and electrical energy when this desorption step is achieved by evacuating the adsorber to a subatmospheric pressure level. Loss of less selectively adsorbed components (often the desired primary product in a PSA process), which remain as coadsorbed and void gas (intra- and interparticle) within the adsorber at the end of the adsorption step, during the depressurization steps, decreases separation efficiency (lower product recovery).

The purge step also lowers the product recovery because a part of the product gas, which is enriched in the less strongly adsorbed components of the feed gas mixture, is typically used as the purge gas. The purge step also dictates the purity of the product gas during the subsequent adsorption step of the process because the purge gas cleans the product end of the adsorber by pushing the concentration fronts of the more strongly adsorbed components toward the feed end. The amount of purge gas used in a PSA process is determined by the extent of desorption of the more strongly adsorbed components during this step and by the extent of product-end cleanup necessary for obtaining the desired working capacity for the more strongly adsorbed components in the PSA cycle at a given product purity. The amount of purge gas required is determined by the capacity, the selectivity, and the strength of adsorption of the more strongly adsorbed components as well as by the conditions of operation (pressure, temperature, and purge gas composition) of the purge step.

The desorption steps often dictate the selection of an adsorbent for a given separation need because they determine the separation efficiency as well as the energy of separation of a PSA process. There is, however, a serious lack of systematic experimental studies of the desorption processes in the adsorption literature. The purpose of this work is to experimentally evaluate different aspects of desorption of pure carbon dioxide by purge with various less selectively adsorbed gases (H_2, N_2, and CH_4) using a set of activated carbons (RB, BPL, and MSC V) and zeolites (NaX and 5A) as adsorbents.

Experimental Methods

Figure 1 shows a schematic diagram of the apparatus used for measuring desorption by purge. It consisted of a stainless steel adsorption column of 1.38 cm internal diameter with a welded stainless steel water jacket (A). The packed height of the adsorbent in the column was 73.7 cm. Pure carbon dioxide or a purge gas could be introduced into the column through flow control valves (C1 or C2) and the three way valve (T1). A gas flow meter (F) measured the flow rate of gas into the column. The effluent gas from the column could either be vented through a control valve (C3) and a three way valve (T2) or sent to a dry test meter (DTM) through a control valve (C4). The DTM measured the cumulative volume of gas leaving the column as a function of time. A small portion of the effluent gas from the column could be diverted to a gas chromatograph for analysis using a control valve (C7). A vacuum pump (V) could also be used to maintain a constant subatmospheric pressure level within the column during the purge step by controlling valves C_2, C_5, and C_6 while keeping valve C_4 closed. The vacuum pump effluent could be sent to

* Author for correspondence.

0888-5885/95/2634-2881$09.00/0

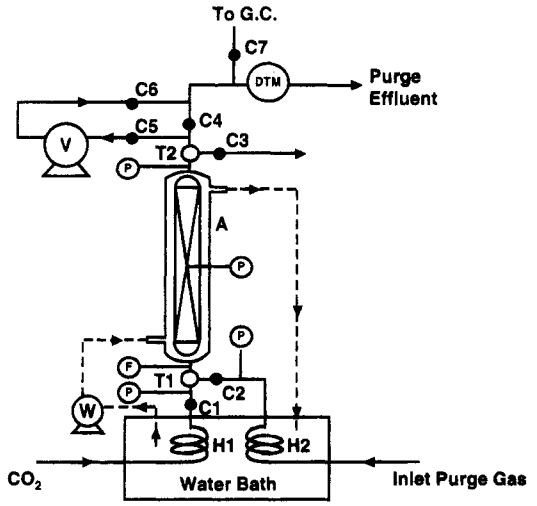

Figure 1. Schematic of experimental apparatus.

the DTM and the gas chromatograph. Pressure gauges (P) were used to monitor the column inlet and effluent gas pressures as well as the midpoint pressure within the column during experiments. A liquid pump (W) was used to circulate water through the column jacket from a constant temperature water bath in order to maintain the column temperature constant during the experiment. Submerged coils (H_1 and H_2) in the water bath were used to preheat the inlet gases to the column to the temperature of the experiment.

The experiment consisted of saturating the regenerated adsorbent in the column with pure CO_2 at a pressure of 1.0 atm and a temperature of 30–65 °C (±0.5 °C) by flowing pure CO_2 through valves C_1 and C_3. Then the pure purge gas (H_2, N_2, or CH_4) was passed through the column by opening valves C_2 and C_4 (C_1, C_3, C_5, and C_6 closed) at a predesigned flow rate. The purge gas was at a pressure of 1.0 atm and a temperature of 30–65 °C. The total effluent gas quantity [$N(t)$] and composition of CO_2 [mole fraction, $y_{CO_2}(t)$] were monitored as functions of time (t) until the CO_2 concentration in the effluent gas was virtually nil. The experiments were repeated using different adsorbents, different purge gas flow rates, and different system temperatures.

Experiments were also conducted where the column pressure was lowered to a subatmospheric pressure (250–760 Torr) level immediately at the start of the purge by using the vacuum pump and by opening valves C_2, C_5, and C_6 (valves C_1, C_3, and C_4 closed). The column pressure was maintained constant at the subatmospheric level during the entire purge process by controlling valves C_5 and C_6. The quantity and the composition of the exit gas from the vacuum pump were measured as functions of time using the DTM and the gas chromatograph.

The adsorption isotherms of pure CO_2, CH_4, and N_2 on different adsorbents at 30 °C (pressure range of 0.01–5.0 atm) and those for pure H_2 at 30 °C (pressure range of 1.0–60.0 atm) were measured using a conventional volumetric adsorption apparatus (Golden and Sircar, 1994).

The activated carbon adsorbents were regenerated by heating in dry N_2 at 150 °C for 8 h. The zeolites were regenerated by heating at a temperature of 300 °C for the same period of time. They were cooled and transferred to the adsorbent column of Figure 1 in a glovebox under dry N_2. The adsorbed and void gas N_2 was

Table 1. Physical Properties of Adsorbents

	BPL carbon	RB carbon	MSC V carbon[a]	5A zeolite[b]	NaX zeolite[c]
BET area (m^2/g)	1100	1250			
pore volume (cm^3/g)	0.70	1.22	0.33	0.42	0.45
skeleton density (g/cm^3)	2.10	2.35	1.93	2.33	2.24
bulk density (g/cm^3)	0.48	0.41	0.71	0.64	0.61
fraction of pore volume below 30 Å diameter	0.57	0.36	0.45	0.32	0.30

[a] MSC V is a molecular sieve carbon with predominately 5 Å micropores. [b] Nominal uniform crystal pore diameter of 5 Å. [c] Nominal uniform crystal pore diameter of 10 Å.

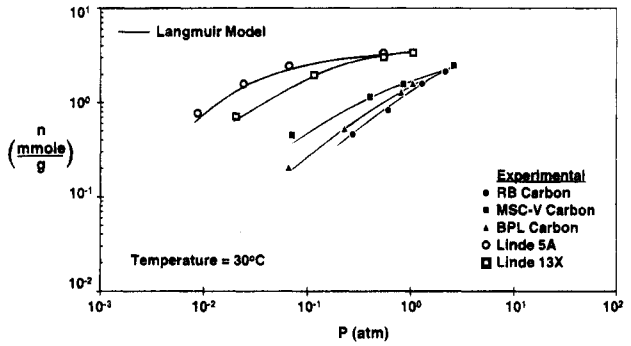

Figure 2. CO_2 adsorption isotherms at 30 °C on various adsorbents.

displaced out of the adsorbent column by CO_2 at the conditions of the purge experiment.

The activated carbons and the zeolites chosen for this study were manufactured by Calgon and Union Carbide Corporations, respectively. They provided a very large spectrum of mean pore opening, pore size distribution, pore volume, BET surface area, as well as surface polarity for adsorption of CO_2 and the purge gases. Table 1 summarizes some of the physical properties of the adsorbents which were obtained from the manufacturer's literature. The activated carbons ranged from a very narrow mean pore size (5 Å) and distribution (MSC V) to a medium mean pore size (~20 Å) and distribution (BPL) to a very large mean pore size (>30 Å) and distribution (RB). The zeolites offered very uniform but distinctly different pore openings (5 and 10 Å) and crystal structures. The activated carbons were used in a granular form (4 × 10 mesh) while the zeolites were pelletized (1/16 in. diameter) beads.

Experimental Results and Data Analysis

Equilibrium Adsorption. The measured pure gas adsorption isotherms are shown in Figures 2 and 3. Figure 2 shows that CO_2 is adsorbed more strongly on the highly polar zeolites than on the less polar carbons as expected. The strength of adsorption and adsorption capacity at any given partial pressure of CO_2 decreased in the order 5A > NaX > MSC V > BPL > RB. Adsorbents with smaller pore sizes in both categories exhibited a higher strength of adsorption for CO_2 as expected. All CO_2 isotherms were type I by the Brunauer classification. Figure 3, on the other hand, shows that H_2 is very weakly adsorbed on all adsorbents even though there is substantial difference between the actual H_2 adsorption capacities on the adsorbents at a given partial pressure. The isotherms were nearly linear in the pressure range of the data. Figure 3 also shows the adsorption isotherms of CH_4 and N_2 on the BPL carbon. They are type I isotherms, and CH_4 is more strongly adsorbed than N_2.

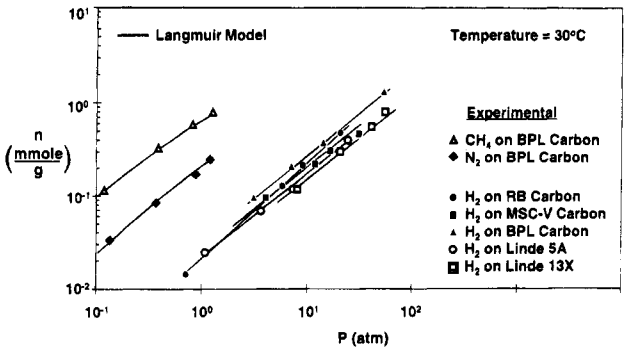

Figure 3. N_2, CH_4, and H_2 adsorption isotherms at 30 °C on various adsorbents.

Table 2. Pure Gas Langmuir Parameters

adsorbent	gas	m (mol/kg)	$b_i^0 \times 10^4$ (atm^{-1})	q_i^0 (kcal/mol)	K_i ((mol/kg)/atm)
BPL	CO_2	3.65	2.80	4.9	3.50
	CH_4	3.65	1.50	4.7	1.35
	N_2	3.65	13.51	2.5	0.31
	H_2	3.65	0.50	3.3	0.044
RB	CO_2	5.00	1.90	4.6	1.98
	H_2	5.00	1.00	2.4	0.027
MSC V	CO_2	2.94	0.02	8.1	4.10
	H_2	2.94	0.80	2.5	0.015
5A	CO_2	3.66	0.10	8.9	96.3
	H_2	3.66	1.60	2.1	0.019
NaX	CO_2	3.70	0.09	8.5	45.1
	H_2	3.70	2.50	1.8	0.018

All isotherms of Figures 2 and 3 can be described by the pure component Langmuir model:

$$n_i^0 = \frac{mb_iP^0}{1 + b_iP^0} \qquad \text{constant } T \tag{1}$$

$$b_i = b_i^0 \exp[q_i^0/RT] \tag{2}$$

Where n_i^0 is the specific amount (mol/kg) of pure gas i adsorbed at pressure P^0 (atm) and temperature T. m is the Langmuir saturation adsorption capacity (mol/kg) for the adsorbate, and b_i (atm^{-1}) is the gas–solid interaction parameter for component i. b_i is a function of temperature given by eq 2. q_i^0 is the isosteric heat of adsorption (cal/mol) of the pure gas, and b_i^0 is a constant. R is the gas constant.

The solid lines of Figures 2 and 3 show the best fit of the experimental data by eq 1. Table 2 gives the model parameters. b_i^0 and q_i^0 were obtained by using experimentally measured isotherms at 30 and 70 °C (not reported here) and fitting them by eqs 1 and 2. The same values of m could be used to describe the adsorption of different gases on the same adsorbent so that the mixed gas Langmuir model can be used to describe binary gas adsorption:

$$n_i = \frac{mb_iPy_i}{1 + \sum b_iPy_i} \qquad \text{constant } T \tag{3}$$

n_i is the specific amount (mol/kg) of component i adsorbed from a mixed gas (mole fraction y_i) at total gas phase pressure P and temperature T. The Langmuirian selectivities of adsorption ($S = b_1/b_2$) for binary pairs [CO_2(1)–purge gas(2)] on the adsorbents are given in Table 3.

The Henry's law constants [$K_i = (\delta n_i^0/\delta P)_T$ at $P \to 0$] for pure gas adsorption on the adsorbents, according to the Langmuir model [$K_i = mb_i$], are also given in Table 2. They quantitatively show that the strength of adsorption of CO_2 on the adsorbents decrease in the order 5A > NaX > MSC V > BPL > RB. The isosteric heats of adsorption for CO_2 on these adsorbents also confirm that order. There are substantial differences between the K_i values for adsorption of CO_2 on the two zeolites (5A > NaX) and the three carbons (MSC V > BPL > RB). CO_2 is very selectively adsorbed over H_2 on all adsorbents. The truly microporous adsorbents (MSC V, 5A, and NaX), however, show exceptionally high selectivities of adsorption of CO_2. Another key difference is the selectivity of adsorption between CO_2 and the purge gases on BPL carbon. They decrease significantly in the order H_2 > N_2 > CH_4.

Table 3. Langmuirian Selectivities of CO_2 over Purge Gases at 30 °C

	Langmuirian selectivity				
binary	RB	BPL	MSC V	NaX	5A
CO_2–H_2	73.4	79.8	273.0	2443.5	5013.4
CO_2–N_2		11.2			
CO_2–CH_4		2.6			

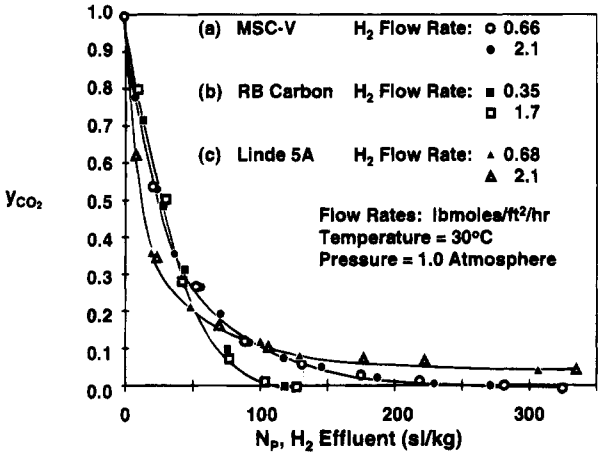

Figure 4. CO_2 desorbed by purging with H_2 at various flow rates from 5A zeolite and MSC V and RB carbons at 1 atm and 30 °C.

Desorption by Purge. The total quantity of CO_2 [$N_{CO_2}(t)$] leaving the adsorbent column (mol/kg) at any time (t) during the purge experiment is given by

$$N_{CO_2}(t) = \int_0^{N(t)} y_{CO_2}(t)\, dN(t) \tag{4}$$

$N(t)$ is the total quantity of column effluent (mol/kg) gas at time t. The total quantity of purge gas [$N_p(t)$] leaving the column at time t (mol/kg) is obtained from

$$N_p(t) = N(t) - N_{CO_2}(t) \tag{5}$$

Figure 4 (curves a–c) shows three typical experimental results for desorption of CO_2 by purge with H_2. They plot $y_{CO_2}(t)$ against $N_p(t)$ at any given time t. $N_p(t)$ is given as standard liters of purge gas leaving the column (1 atm, 21 °C) per kilogram of adsorbent. The plots of Figure 4 correspond to the adsorbents MSC V carbon (a), RB carbon (b), and 5A zeolite (c) which represent the spectrum of large and small pore adsorbents as well as adsorbents with very high and low strengths of adsorption for CO_2. Two purge gas inlet flow rates differing by a factor of 3 were used in each of these tests. The data of Figure 4, however, show that the flow rate had no effect on the desorption characteristics of CO_2. This indicates that adsorbate mass transfer rates were

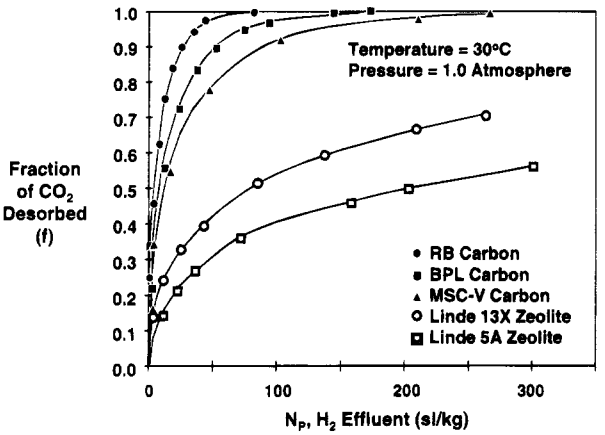

Figure 5. Fractional CO_2 desorption by purging with H_2 at 30 °C from BPL, MSC V, and RB carbons and Linde 5A and 13X zeolites.

not limiting for these desorption processes and local equilibrium between gas and adsorbed phases prevailed within the adsorber for the flow rate range of the data. Local equilibrium was attained irrespective of the large differences in adsorbent pore sizes and affinity of adsorption of CO_2 by these adsorbents. The quantity of purge gas needed to clean the column was, however, a strong function of the strength of adsorption of CO_2. This quantity decreased in the order 5A > MSC V > RB as expected.

Efficiency of Desorption by Purge

The efficiency of desorption by purge can be defined by the quantity of purge gas $[N_p(y)]$ lost in the column effluent in order to desorb the adsorbed component. This quantity is a function of effluent gas composition (y). The lower this quantity for a given desorption duty, the more efficient is the desorption by purge. Figure 5 shows the fraction (f) of total CO_2, originally present in the adsorption column (adsorbed and void gas), that is removed from the column by purging with H_2 when the cumulative purge gas quantity in the effluent gas is N_p. It shows that complete CO_2 desorption ($f = 1$) from the RB carbon can be achieved when N_p is 80 sL/kg (standard liters per kilogram). The f values for BPL and MSC V carbons and NaX and 5A zeolites at that value of N_p are, respectively, 0.96, 0.88, 0.5, and 0.37. In other words, the RB carbon, which adsorbs CO_2 least strongly among these adsorbents, provides the most efficient desorption by purge with H_2. The efficiency of desorption by purge at any given f value decreases in the order RB > BPL > MSC V > NaX > 5A. The zeolites, in general, are very inefficient adsorbents for desorption of CO_2 by purge compared to the activated carbons. This characteristic alone often favors the use of activated carbons in a practical PSA process where bulk CO_2 has to be removed from a feed gas, even though zeolites may offer larger adsorption capacities for CO_2 (Figure 2). An example of such case is production of pure H_2 from steam–methane-reformer off-gas by PSA (Wagner, 1969; Fuderer and Rudelstorfer, 1976; Sircar, 1979).

It should be noted that the $N_p(y)$ profiles of Figure 5 are determined by the shape of the isotherm of the component being desorbed as well as by that of the purge gas. For Langmuir isotherms, the isotherm parameters given in Table 2 define these shapes.

Among the three carbons tested, the RB and BPL carbons provide much better efficiency for desorption

Table 4. Total CO_2 Capacity of Adsorbent Columns at 1.0 atm and 30 °C

adsorbent	evaluated from equilibrium isotherms (mol/kg)	obtained from purge experiment (mol/kg)
BPL	1.93	2.05 (purge by H_2)
		1.96 (purge by N_2)
		1.89 (purge by CH_4)
RB	1.39	1.48 (purge by H_2)
MSC V	1.82	1.81 (purge by H_2, 1 atm)
		1.77 (purge by H_2, 0.66 atm)
		1.78 (purge by H_2, 0.33 atm)
5A	3.52	
NaX	3.69	

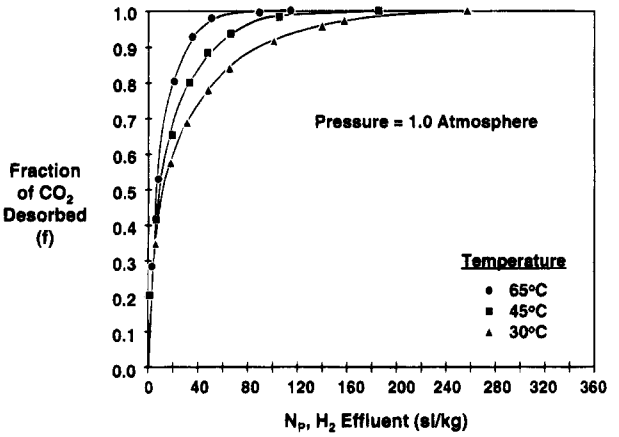

Figure 6. Effect of temperature on fractional CO_2 desorption by purging with H_2 at 30 °C from MSC V carbon.

of CO_2 by purge than the MSC V carbon, even though the latter has a higher selectivity of adsorption of CO_2 over H_2.

Table 4 shows the total CO_2 capacity (adsorbed and void) at atmospheric pressure and 30 °C on the adsorbents of this study. The void gas quantity of CO_2 (mol/kg of adsorbent) in the column at the start of purge test was calculated by $\{\varrho_g [1/\varrho_s - 1/\varrho_c]\}$. ϱ_g, ϱ_s, and ϱ_c are, respectively, the density of gaseous CO_2 at the pressure and temperature of the experiment and the bulk and the skeleton densities of the adsorbent (Table 1). The first column of Table 4 gives the total specific CO_2 capacity of the column calculated using the adsorption isotherms of Figure 2 and the void gas quantities. The second column of Table 4 was calculated by integrating the complete $y_{CO_2}(t)$–$N(t)$ plots (eq 4) for the purge tests. These results show that the total quantity of CO_2 desorbed during the purge tests compares extremely well with that obtained independently by equilibrium measurements.

Effect of Temperature

Figure 6 shows the effect of adsorbent temperature on the efficiency of desorption by purge. It plots the fraction (f) of CO_2 desorbed from MSC V carbon by H_2 purge as a function of N_p at 30, 45, and 65 °C. 98% of CO_2 is desorbed ($f = 0.98$) from the carbon at a N_p value of 60 sL/kg when the adsorbent temperature was 65 °C. The corresponding f values at 45 and 30 °C are, respectively, 0.92 and 0.83. Clearly, higher temperature facilitates desorption of CO_2 from the carbon because it is held less strongly (smaller b_1). Higher temperature also decreases the adsorption capacity of CO_2 and its selectivity over H_2. However, the increase in efficiency of desorption by purge at a higher temperature may

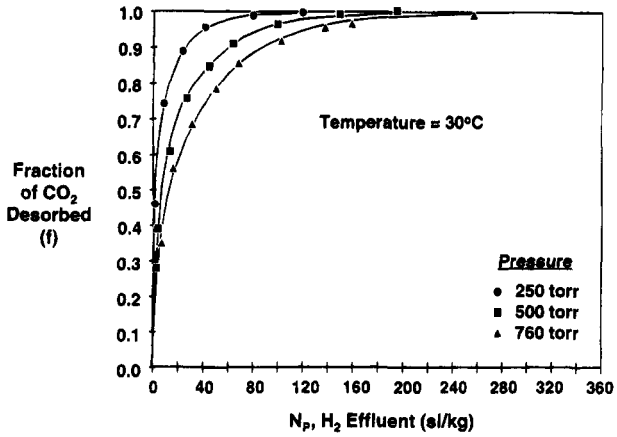

Figure 7. Effect of pressure on fractional CO_2 desorption by purging with H_2 at 30 °C from MSC V carbon.

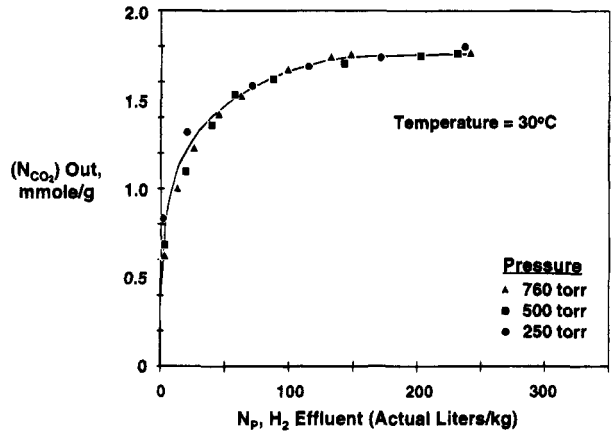

Figure 8. CO_2 (1 atm and 30 °C) desorption by purging with H_2 (P and 30 °C) at various pressures plotted in terms of actual volume of effluent purge gas.

justify operation of a PSA process at an elevated temperature due to better separation efficiency. This principle was used in the design of a PSA air separation process at an elevated temperature (Sircar, 1982).

Effect of Purge Gas Pressure

Figure 7 shows the fractions of CO_2 desorbed (f) from a MSC V carbon column saturated with pure CO_2 at 1.0 atm and 30 °C and subsequently purged with pure H_2 at constant column pressures (P) of 0.33, 0.66, and 1.0 atm. The quantity (N_p) of H_2 purge gas lost (sL/kg at 1.0 atm and 30 °C) in order to obtain a certain value of f decreases significantly when the purge gas pressure is reduced. The total specific amount of CO_2 desorbed from the column is same in all cases (Table 4).

The data of Figure 7 are replotted in Figure 8 in terms of the total moles of CO_2 desorbed as a function of actual volume of H_2 lost (L/kg at P and 30 °C) at the pressure of purge. Figure 8 shows that the data of Figure 7 collapse into a single line. This result demonstrates a fundamental concept used in PSA process design that the efficiency of desorption by a purge process is determined by the actual volume of purge gas used at the conditions (pressure and temperature) of purge. The loss of purge gas can be minimized by carrying out the purge step at the lowest practical pressure level permitted by the process design. This principle has been incorporated in many PSA process designs where the purge step is carried out under subatmospheric pressure conditions (Haruna et al., 1990).

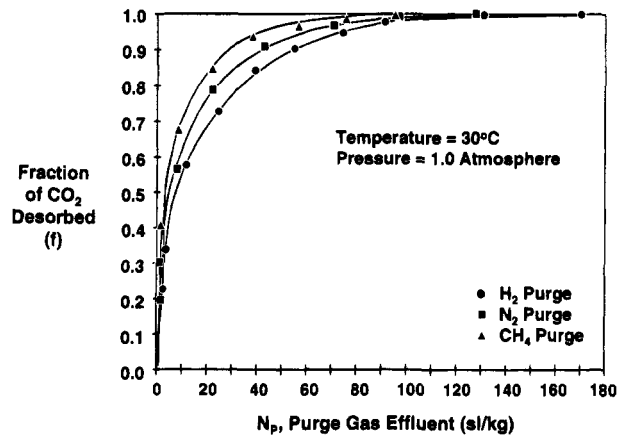

Figure 9. Effect of purge gas properties on fractional CO_2 desorption from BPL carbon at 30 °C.

Effect of Purge Gas Selectivity

Figure 9 shows the fractional desorption of CO_2 (f) from BPL carbon by purging with pure H_2, N_2, and CH_4. The selectivity of adsorption of CO_2 over these purge gases decreases in the order $H_2 > N_2 > CH_4$ (Table 3). The figure shows that the quantity of purge gas lost decreases as the selectivity of adsorption between the more strongly adsorbed component and the purge gas decreases. This characteristic may be used in the selection of a purge gas (when a choice is available) in order to enhance the separation efficiency of a PSA process. This concept was used in the design of a PSA process for production of ammonia synthesis gas from SMR off-gas (Sircar, 1989b).

The above described experimental results demonstrate the key characteristics of the desorption process by purge. They may be judiciously used in designing the purge step of a PSA process for improving overall separation efficiency as well as for selection of the optimum adsorbent and purge gas for a given separation.

Local Equilibrium Theory of Desorption by Purge

A very general model of adiabatic desorption by purge under local equilibrium conditions has already been developed (Sircar and Kumar, 1985). The experimentally observed characteristics of desorption by purge reported in this work were predicted by the model. Here, we further develop the mathematical framework for the special case of isothermal–isobaric desorption by purge.

The local equilibrium theory assumes that the adsorbate in the bulk gas phase in the adsorber is at instantaneous thermodynamic equilibrium with the adsorbed phase. Every fluid element in the gas phase is characterized by a composition (mole fraction of component i: y_i), a mass flow rate ((mol/ft^2 of empty cross section of adsorber)/s: Q), and the constant pressure (P) and temperature (T) of the system. The adsorbed phase is characterized by a specific adsorbate loading for each component i (mol/kg: n_i) which is in equilibrium with the gas phase at P, T, and y_i.

For a binary adsorption system, where the gas phase mole fraction of the more strongly adsorbed species (component 1) is given by y, the isothermal–isobaric

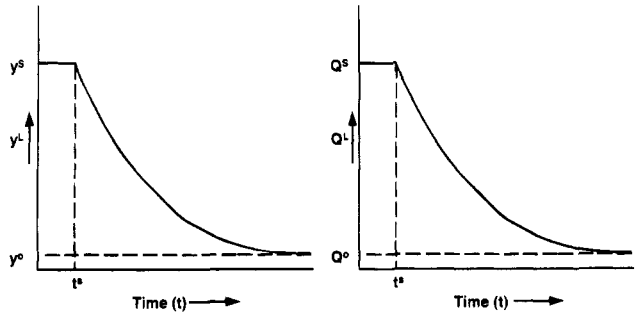

Figure 10. Characteristic column effluent profiles (flow and composition) for desorption by purge.

local equilibrium theory yields (Sircar and Kumar, 1985):

$$\frac{\mathrm{d}\ln Q(y)}{\mathrm{d}y} = \frac{\varrho_s n_y}{\epsilon\varrho_g + \varrho_s[n_{1y} - y n_y]} \tag{6}$$

$$\beta(y) = \frac{Q(y)}{\epsilon\varrho_g + \varrho_s[n_{1y} - y n_y]} \tag{7}$$

where $\beta(y)$ is the characteristic velocity (cm/s) of the fluid element of composition y. ϱ_s and ϱ_g are, respectively, the adsorbent bulk density (g/cm^3) and the gas phase molar density (mol/cm^3). ϱ_g is equal to (P/RT) for an ideal gas. R is the gas constant. ϵ is the helium void fraction of the adsorber. n_{1y} [$= (\delta n_1/\delta y)_{P,T}$], n_{2y} [$= (\delta n_2/\delta y)_{P,T}$], and n_y [$= \Sigma n_{iy}$] are slopes of binary adsorption isotherms at constant total gas phase pressure and system temperature.

Consider an isobaric–isothermal purge experiment where the adsorber [length L, cross sectional area A, volume V ($=AL$), weight of adsorbent W ($=V\varrho_s$)] is initially saturated with a binary gas mixture at P, T and y^s and then purged with a binary gas stream at P, T, and y^0 ($< y^s$). The purge gas mass flow rate (Q^0) at the inlet is kept constant. The column effluent composition (y^L) and mass flow rate (Q^L) vary with time (t) according to the schematic of Figure 10. y^L and Q^L remain constant at values of y^s and Q^s for a finite period of time (t^s). Then they gradually change with time to approach y^0 and Q^0, respectively. The total specific amounts (mol/kg) of component i (=1, 2) leaving the column (N_i) at time t (when effluent gas composition is y) are given by

$$N_1(y) = \frac{A}{W}\int_0^t Q^L y^L\,\mathrm{d}t = N_1^s + \frac{A}{W}\int_{t^s}^t Q^L y^L\,\mathrm{d}t \tag{8}$$

$$N_2(y) = \frac{A}{W}\int_0^t Q^L(1 - y^L)\,\mathrm{d}t = N_2^s + \frac{A}{W}\int_{t^s}^t Q^L(1 - y^L)\,\mathrm{d}t \tag{9}$$

where N_1^s ($=AQ^s y^s t^s/W$) and N_2^s ($=(AQ^s(1 - y^s)t^s)/W$) are specific cumulative amounts (mol/kg) of components 1 and 2 leaving the column at time t^s.

For a binary Langmuirian adsorbate system, eqs 1–7 can be combined and integrated to obtain

$$\frac{Q(y)}{Q^0} = \left[\frac{(Z - \beta_1)(Z_0 - \beta_2)}{(Z - \beta_2)(Z_0 - \beta_1)}\right]^C \tag{10}$$

$$\frac{\beta(y)}{\beta^0} = \left[\frac{Z - \beta_1}{Z_0 - \beta_1}\right]^{(C-1)}\left[\frac{Z_0 - \beta_2}{Z - \beta_2}\right]^{(C+1)}\left(\frac{Z}{Z_0}\right)^2 \tag{11}$$

$$\beta^0(y^0) = \frac{Q^0(y^0)(Z_0^2)}{\alpha(m\varrho_s)(Z_0 - \beta_1)(Z_0 - \beta_2)} \tag{12}$$

$$Z = (1 + b_2P) + (b_1 - b_2)Py = (1 + b_2P)(1 + \lambda y) \tag{13}$$

$$\lambda = \frac{(b_1 - b_2)\,P}{(1 + b_2\,P)} \tag{14}$$

$$S = b_1/b_2 \tag{15}$$

$$\beta_1 = \frac{1 + \sqrt{1 - 4\alpha\psi}}{2\alpha};\quad \beta_2 = \frac{1 - \sqrt{1 - 4\alpha\psi}}{2\alpha} \tag{16}$$

$$C = \frac{1}{\sqrt{1 - 4\alpha\psi}} \tag{17}$$

$$\psi = (1 + b_1P)(1 + b_2P) \tag{18}$$

$$\alpha = [\epsilon\varrho_g/m\varrho_s] \tag{19}$$

Z_0 and Z_s correspond to the values of Z given by eq 13 when y is equal to y^0 and y^s, respectively. S is the selectivity of adsorption of component 1 over component 2.

The total specific quantities (mol/kg) of component i in the adsorber at the start of purge are

$$\bar{n}_1 = my^s\left[\alpha + \frac{S\lambda}{(S - 1)(1 + \lambda y^s)}\right] \tag{20}$$

$$\bar{n}_2 = m(1 - y^s)\left[\alpha + \frac{\lambda}{(S - 1)(1 + \lambda y^s)}\right] \tag{21}$$

The specific effluent quantities (mol/kg) are given by

$$N_1^s = \bar{n}_1 - \frac{m\lambda(\lambda + 1)(y^s)^2}{(1 + \lambda y^s)^2} \tag{22}$$

$$N_2^s = \bar{n}_2 + \frac{m\lambda(1 - y^s)^2}{(1 + \lambda y^s)^2} \tag{23}$$

$$N_1(y) = \bar{n}_1 - \frac{m(1 + \lambda)}{\lambda}\left[1 - \left\{\frac{1 + 2\lambda y}{(1 + \lambda y)^2}\right\}\right] \tag{24}$$

$$N_2(y) = \bar{n}_2 + \frac{m}{\lambda}\left[1 - \left\{\frac{(1 + \lambda)[1 - \lambda(1 - 2y)]}{(1 + \lambda y)^2}\right\}\right] \tag{25}$$

The specific quantity (mol/kg) of purge gas (N^p) introduced into the adsorber (when the effluent gas composition is y) is given by

$$N^p = \int_0^t \frac{AQ^0}{W}\,\mathrm{d}t = \frac{(m\alpha)(Z - \beta_1)(Z - \beta_2)}{Z^2}\left[\frac{(Z - \beta_2)(Z_0 - \beta_1)}{(Z - \beta_1)(Z_0 - \beta_2)}\right]^C \tag{26}$$

The fraction (f) of component 1 present in adsorber at the start of the purge process, which is removed from the adsorber (when the effluent gas composition is y), is given by

$$f(y) = \frac{N_1(y)}{\bar{n}_1} \tag{27}$$

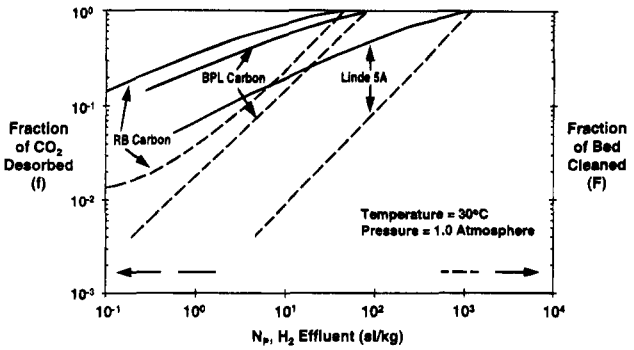

Figure 11. Plots of fraction of CO_2 desorbed (f) by purging with H_2 and the corresponding fraction of bed cleaned (F) for various adsorbents.

$f(y)$ and the corresponding loss of component 2, $[N_2(y)]$, can be calculated using eqs 20–27. A plot of $f(y)$ against $N_2(y)$ as shown by Figures 5–9 defines the efficiency of the purge process as discussed earlier. The quantity $N_2(y)$ was previously referred to as N_p when the column was initially saturated with pure component 1 and then purged with pure component 2.

Another very important property defining the efficiency of desorption by purge process is the fraction of adsorption column (F) at the purge inlet end which becomes free of saturating gas at the start of this process. This section of the column is saturated with the purge inlet gas at P, T, and y^0 at the end of the purge step . For the special case when the purge gas is free of component 1 ($y^0 = 0$), this cleaned section is completely free of component 1. The larger the value of F is, the more efficient the desorption by purge process is. The present model yields the following expression for $F(y)$ when the purge effluent gas composition is y:

$$F(y) = \left[\frac{Z_0 - \beta_1}{Z - \beta_1}\right]^{(C-1)}\left[\frac{Z - \beta_2}{Z_0 - \beta_2}\right]^{(C+1)}\left(\frac{Z_0}{Z}\right)^2 = \frac{\beta^0}{\beta(y)} \quad (28)$$

Equations 8–28 provide a complete set of analytical solutions for describing the isothermal–isobaric purge process for a binary Langmuirian system. Approximate analytical expressions for $Q(y)$ and $\beta(y)$ were previously obtained (Sircar and Kumar, 1985) from eqs 6 and 7 for the special case of $\epsilon\varrho_g \ll \varrho_s\,[n_{1y} - yn_y]$.

Figure 11 shows plots of $F(y)$ and $f(y)$ against H_2 purge effluent quantity for desorption of pure CO_2 from three different adsorbents. The Langmuir parameters (Table 2) were used for these calculations using eqs 26, 27, and 28. It shows that the fraction of column cleaned (free of CO_2) during purge (F) decreases drastically for a given quantity of H_2 effluent as the strength of adsorption of CO_2 and its selectivity over the purge gas component increases (5A > BPL > RB). The fraction of CO_2 desorbed (f) follows the same trend. However, at a given H_2 purge effluent quantity, the fraction of CO_2 desorbed (f) far exceeds the fraction of the bed cleaned for all adsorbents. For example, at a H_2 purge effluent quantity of 10 sL/kg, the fractions of CO_2 (f) desorbed from RB, BPL, and 5A are 64%, 56%, and 19%, respectively. The corresponding values for the fraction of the bed cleaned (F) for these three adsorbents are only 23%, 14%, and 0.84%. The importance of the fraction of the bed cleaned (F) during the purge step is crucial in determining the overall separation efficiency by the PSA process. For the present case, it determines the position of the residual CO_2 zone in the column at the end of the purge step which subsequently dictates the CO_2

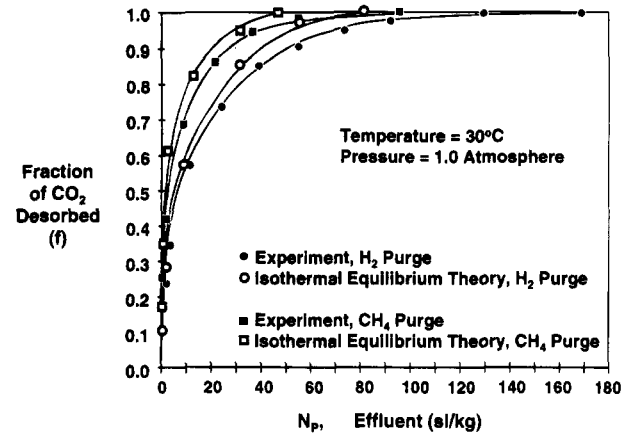

Figure 12. Comparison of experiment and local equilibrium theory calculations for CO_2 desorption by purging with H_2 and CH_4 from BPL carbon at 30 °C.

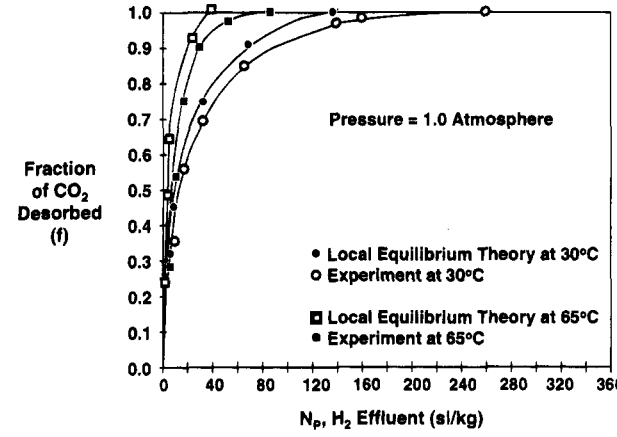

Figure 13. Comparison of experiment and local equilibrium theory calculations for CO_2 desorption by purging with H_2 on MSC V at two temperatures.

breakthrough time for any CO_2 containing feed gas. Thus, the quantity F provides a very valuable tool for fully understanding the efficiency of desorption by purge. The efficiency of desorption estimated by the quantity f alone is not sufficient.

The total quantity of pure purge gas $[y^0 = 0, Z_0 = (1 + b_2P)]$ required to completely clean the column $[y = 0, Z = (1 + b_2P)]$ can be obtained from eq 26:

$$N^p[y^0 = 0, y = 0] = n_2^0(P)S \quad (29)$$

$n_2^0(P)$ is the specific adsorption capacity (eq 1) of pure purge gas at P and T. Equation 29 shows that the purge gas quantity to completely clean the column is decreased when (a) the total gas pressure (P) is reduced [lower $n_2^0(P)$] and (b) the selectivity of adsorption of component 1 over component 2 (S) is low. It can be shown from eq 26 that the same conclusions are valid even for partial cleaning of the column by purge. Our experimental data for desorption of CO_2 from BPL carbon by purge at different pressures (Figures 7 and 8) and by purge with H_2, N_2, and CH_4 (Figure 9) exhibit these characteristics.

Figures 12 and 13 show several comparisons between the calculated fractional desorption (f) of CO_2 (eqs 20, 24, and 27) as functions of the purge gas effluent quantity (eq 26) and experimental data. Desorption of pure CO_2 from BPL carbon by purging with pure H_2 and CH_4 at 303 K (Figure 12) and desorption of pure CO_2 from MSC V carbon by purging with H_2 (Figure 13) at

303 and 338 K are shown. The isothermal local equilibrium model describes the experimental desorption characteristics very well up to a very high level of fractional desorption of CO_2 ($f \leq 0.8$) in all cases. The experimental purge gas effluent quantity is consistently larger than the model calculations in the final section ($f > 0.8$) of the desorption profile. A possible explanation for this behavior is that the adsorption column may not be truly isothermal during the process. It was theoretically demonstrated that adiabatic columns require a larger amount of purge gas in order to remove the final portion of the adsorbed component (Sircar and Kumar, 1985). The change in the adsorbent temperature for supplying the heat of desorption by purge can be very large in an adiabatic column. For example, the adsorbent temperature can change from 300 to 263 K during adiabatic desorption of pure CO_2 by purge with pure H_2 (mass flow rate = 5.0 (lb mol/h)/ft^2) at a total gas phase pressure of 1.0 atm. The corresponding change of adsorbent temperature by purge with pure CH_4 is only 287 K. The water-jacketed system of the present study may have failed to instantaneously supply the heat to the adsorbent in order to obtain perfect isothermality.

Summary

Experimental evaluation of isothermal desorption of CO_2 from various microporous adsorbents by purging with H_2, N_2, and CH_4 showed that the desorption process is governed by local equilibrium between gas and adsorbed phases when the purge gas flow rates are moderate.

The loss of purge gas during the desorption process is reduced by operation at lower total gas pressure and higher adsorbent temperature, as well as by decreasing the selectivity of adsorption between the adsorbate being desorbed and the purge gas.

The efficiency of the desorption process is determined by (i) the amount of purge gas lost in order to remove a certain fraction of the more selectively adsorbed component and (ii) the fraction of clean adsorber volume generated at the purge inlet side during that process.

The selection of an adsorbent for a given separation process may be dictated by the efficiency of desorption by purge. Adsorbents with a high strength of adsorption for the selectively adsorbed components may not be preferred due to the larger quantity of purge gas lost and the smaller fraction of clean adsorber volume generated.

The local equilibrium models provide analytical solutions for describing the characteristics of desorption by purge. They can be adequate for first pass design.

Nomenclature

A = empty cross sectional area of adsorber
b = Langmuir gas–solid interaction parameter for pure gas
C = defined by eq 17
f = fraction of more strongly adsorbed component removed during purge process
F = fraction of adsorber free of more strongly adsorbed component at the purge gas inlet end during purge process
K = Henry's law constant for adsorption of pure gas
m = Langmuir saturation adsorption capacity for pure gas
n = specific amount adsorbed
n_y = slopes of binary equilibrium isotherms
N = specific amount of effluent from column during purge process
N_p = Specific amount of purge gas lost during purge process
N^p = Specific amount of purge gas introduced during purge process
P = pressure
Q = mass flow rate through adsorber
q = isosteric heat of adsorption
R = gas constant
S = selectivity of adsorption
T = temperature
t = time
t^s = time during which colum effluent composition remains at y^s
V = volume of adsorber
W = weight of adsorbent in column
y = gas phase mole fraction
Z = defined by eq 13

Greek Letters

α = defined by eq 19
$\beta(y)$ = characteristic velocity of fluid element of composition y
β_1, β_2 = defined by eq 16
λ = defined by eq 14
ψ = defined by eq 18
ϵ = helium void in column
ϱ_g = gas density at P and T
ϱ_s = bulk density of adsorbent
ϱ_c = skeleton density of adsorbent

Subscripts

i = component i

Superscripts

0 = pure gas, purge gas conditions at inlet end of column
s = column saturating gas conditions at start of purge step
L = column effluent gas conditions at the exit end of the column

Literature Cited

Fuderer, A.; Rudelstorfer, E. Selective Adsorption Process. U.S. Patent 3,986,849, 1976.

Golden, T. C.; Sircar, S. Gas Adsorption on Silicalite. *J. Colloid Interface Sci.* **1994**, *162*, 182–188.

Haruna, K.; Ueda, K.; Inoue, M.; Someda. M. Process for Recovering Oxygen Enriched Gas. U.S. Patent 4,917,710, 1990.

Sircar, S. Separation of Multicomponent Gas Mixtures by Pressure Swing Adsorption. U.S. Patent 4,171,207, 1979.

Sircar, S. Air Separation by Pressure Swing Adsorption. U.S. Patent 4,329,158, 1982.

Sircar, S. Pressure Swing Adsorption Technology. *Adsorption: Science and Technology*; Rodriques, A. E., et al., Eds.; NATO Advanced Study Institute Series E; Kluwer Academic Publishers: Dordrecht, The Netherlands, 1989a, Vol. 158, 285–321.

Sircar, S. Recovery of Nitrogen, Hydrogen and Carbon Dioxide from Hydrocarbon Reformate. U.S. Patent 4,813,980, 1989b.

Sircar, S.; Kumar, R. Equilibrium Theory for Adiabatic Desorption of Bulk Binary Gas Mixtures by Purge. *Ind. Eng. Chem. Process Des. Dev.* **1985**, *24*, 358–364.

Wagner, J. L. Selective Adsorption Process. U.S. Patent 3,430,418, 1969.

Received for review January 30, 1995
Revised manuscript received April 17, 1995
Accepted April 21, 1995[⊗]

IE950092E

[⊗] Abstract published in *Advance ACS Abstracts,* July 1, 1995.